Structure
Article

Quaternary Structure of Flavorubredoxin as Revealed by Synchrotron Radiation Small-Angle X-Ray Scattering

Maxim V. Petoukhov,[1,2,4] João B. Vicente,[3,4] Peter B. Crowley,[3,5] Maria Arménia Carrondo,[3] Miguel Teixeira,[3,*] and Dmitri I. Svergun[1,2,*]

[1]European Molecular Biology Laboratory, Hamburg Outstation, Notkestrasse 85, 22603 Hamburg, Germany
[2]Institute of Crystallography, Russian Academy of Sciences, Leninsky pr. 59, 117333 Moscow, Russia
[3]Instituto de Tecnologia Química e Biológica, Universidade Nova de Lisboa, Apartado 127, 2781-901 Oeiras, Portugal
[4]These authors contributed equally to this work
[5]Present address: School of Biomolecular and Biomedical Science, Conway Institute, University College Dublin, Belfield, Dublin 4, Ireland
*Correspondence: miguel@itqb.unl.pt (M.T.), svergun@embl-hamburg.de (D.I.S.)
DOI 10.1016/j.str.2008.06.009

SUMMARY

Flavodiiron proteins (FDP) are modular enzymes which function as NO and/or O_2 reductases. Although the majority is composed of two structural domains, the homolog found in *Escherichia coli*, flavorubredoxin, possesses an extra C-terminal module consisting of a linker and a rubredoxin (Rd) domain necessary for interprotein redox processes. In order to investigate the location of the Rd domain with respect to the flavodiiron structural core, small-angle X-ray scattering was used to construct low-resolution structural models of flavorubredoxin. Scattering patterns from the Rd domain, the FDP core, and full-length flavorubredoxin were collected. The latter two species were found to be tetrameric in solution. Ab initio shape reconstruction and rigid-body modeling indicate a peripheral location for the Rd domains, which appear to have weak contacts with the FDP core. This finding suggests that Rd behaves as an independent domain and is freely available to participate in redox reactions with protein partners.

INTRODUCTION

Flavodiiron proteins (FDP; formerly named A-type flavoproteins; Wasserfallen et al., 1998) constitute a widespread family of nitric oxide and/or oxygen reductases (Vicente et al., 2008) encoded in the genomes of mainly anaerobic bacteria, archaea, and a few protozoan pathogens (Andersson et al., 2006; Saraiva et al., 2004; Sarti et al., 2004). Members of this protein family have been assigned either complementary or alternative NO and O_2 reductase activities, and play important roles in pathogen survival. The family is defined by a common polypeptide sequence of about 400 amino acids that constitute the structural core of these proteins. Crystal structures have been determined for several FDPs (Frazao et al., 2000; Seedorf et al., 2007; Silaghi-Dumitrescu et al., 2005a) (Di Matteo et al., 2008). The first crystallographic structure solved—that of *Desulfovibrio gigas* rubredoxin:oxygen oxidoreductase (Dg_ROO) (Frazao et al., 2000)—revealed that FDP is a fusion of two distinct structural domains, a metallo-β-lactamase domain harboring a diiron site and a flavodoxin domain binding one flavin mononucleotide (FMN) with an ~25 Å separation between the two redox centers. However, Dg_ROO (and so far all FDPs crystallized) was shown to have a head-to-tail homodimeric arrangement in which the diiron center from one monomer is juxtaposed with the FMN of the second monomer (Figure 1B). This quaternary arrangement appears to be essential for a functional FDP, because it allows efficient electron transfer from the electron-accepting FMN group to the diiron active site where reduction of NO or O_2 takes place (Vicente et al., 2008). In all of the known structures, FDP is dimeric and, with the exception of *Thermotoga maritima* (Protein Data Bank [PDB] ID code 1VME), the crystal packing interfaces suggest the formation of higher-order oligomers such as tetramers (Figure 1B).

Whereas the vast majority of FDPs consist of the two-domain architecture, some members of the family bear extra C-terminal domains with redox-active centers (Figure 1A). Such is the case of *Escherichia coli* flavorubredoxin (FlRd), which has a C-terminal rubredoxin (Rd) module harboring an iron center coordinated by the sulfur atoms of four cysteine residues (Fe-Cys_4). The Rd module is connected to the flavodoxin domain in FlRd by a linker of approximately 20 amino acids. Taking into account that rubredoxin is the redox partner of Dg_ROO (and likely of other FDPs) (Chen et al., 1993; Gomes et al., 1997; Rodrigues et al., 2006; Silaghi-Dumitrescu et al., 2005b; Victor et al., 2003), the fused Rd module in FlRd simplifies the overall electron transfer chain that couples NADH oxidation to NO and/or oxygen reduction (Figure 1) (Gomes et al., 2000, 2002). A combination of redox and kinetics studies has established the Rd domain as the electron-accepting site of FlRd upon interaction with its NADH oxidizing redox partner (Figure 1A) (Vicente et al., 2007; Vicente and Teixeira, 2005). Moreover, these studies demonstrated a modulation of the reduction potentials of FlRd upon formation of an electron transfer complex with its reductase. Thus, to establish the intramolecular electron flow mechanism from the Rd domain to the FMN and diiron cofactors, it remains essential to understand the relative position of the Rd domain with respect to the FDP core of FlRd. Attempts to model FlRd using the known FDP

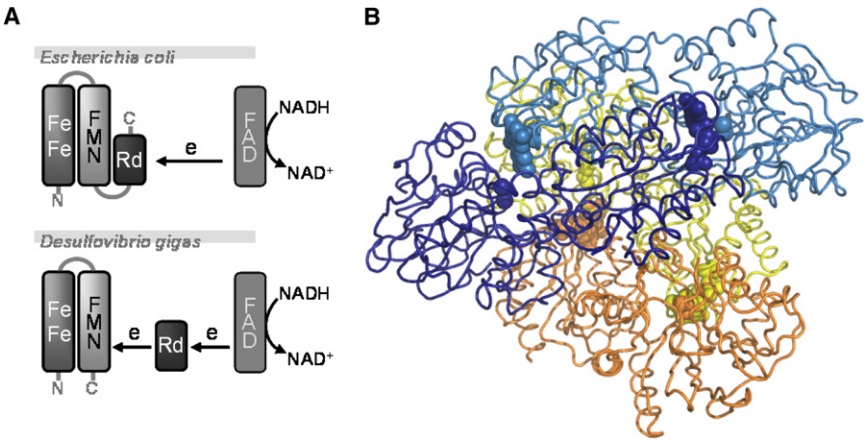

Figure 1. FDP Organization and Electron Transfer

(A) Scheme depicting the electron transfer chains in *E. coli* and *D. gigas* involving FDPs as nitric oxide and/or oxygen reductases. Fe-Fe box, metallo-β-lactamase domain of FDP; FMN box, flavodoxin domain of FDP; Rd box, rubredoxin, an additional module of *E. coli* FDP (flavorubredoxin, FlRd), or a redox partner of *D. gigas* FDP; FAD box, NADH:(flavo)rubredoxin oxidoreductase.

(B) The tetrameric assembly of FDPs as revealed by X-ray crystallography. Note the dimer of dimers arrangement. The chains from one of the dimers are highlighted in dark and light blue with the diiron and FMN groups shown as spheres. The other dimer is colored orange and yellow. The coordinates of *M. thermoacetica* FDP (PDB ID code 1YCH; Silaghi-Dumitrescu et al., 2003) were used to prepare the figure in PyMOL (DeLano, 2002).

and Rd structures have been elusive, as it is difficult to predict how the linker might pack against the FDP core.

The quaternary structure of FlRd, in particular the location of the Rd module, was investigated by synchrotron small-angle X-ray scattering (SAXS). When measuring SAXS from dilute monodisperse macromolecular solutions, the angular dependence of the X-ray scattering intensity is proportional to the scattering from a single particle averaged over all orientations (Feigin and Svergun, 1987). Analysis of the SAXS patterns, using ab initio shape reconstruction or rigid-body modeling, provides information on low-resolution solution structures (Petoukhov and Svergun, 2005). Both full-length FlRd and its truncated constructs (the FDP core lacking the Rd module and the Rd module alone; Table 1) were studied and a structural model of FlRd was constructed providing insight into the quaternary structure of this modular NO reductase.

RESULTS

Overall Parameters

The experimental scattering patterns from the measured constructs are presented in Figure 2A, and the overall structural parameters computed from the SAXS data are given in Table 2. The scattering curve from the homology model of the Rd domain computed by the program CRYSOL (Svergun et al., 1995) agrees well with the experimental data showing only minor deviations (Figure 2A; Table 2), which may be attributed to the fact that the Rd construct contains the linker region (Table 1). Using the forward scattering I_0 of the Rd domain as a reference, the molecular masses (MM) of the FDP core and the full-length FlRd were estimated as 200 and 227 kDa, respectively, pointing to a tetrameric assembly in both cases. This conclusion is further corroborated by the excluded volume V_p. Indeed, the increase in the V_p and I_0 values of FlRd (Table 2) is compatible, within error, with the addition of four copies of the Rd domain with the linker to the FDP core. The much larger maximum size (D_{max}) and radius of gyration (R_g) values of FlRd compared to FDP (Table 2) indicate a peripheral location for the Rd domain in FlRd. The distance distribution functions $p(r)$ of the two constructs (Figure 2B), computed from the experimental data using the indirect Fourier transform program GNOM (Svergun, 1992), further support this finding. The $p(r)$ functions are similar up to intraparticle distances of 4.2 nm but display different profiles at larger distances. The full-length FlRd has a larger maximum size, and its $p(r)$ goes systematically above that of the FDP for distances > 5 nm. Given that each monomer of FlRd contains an FDP flanked by an Rd module, this observation suggests that the arrangement of the monomers in the tetrameric FDP is preserved in full-length FlRd, whereas the Rd domains are located on the periphery.

Table 1. Size of Protein Constructs Investigated by SAXS

Name	Length	MM Monomer (kDa)
FlRd	1–479	~55
FDP	1–412	~47
Rd	401–479	~8.6

Shape Determination

Low-resolution ab initio models of FDP and FlRd were constructed in the bead modeling program DAMMIN (Svergun, 1999). The assumption of P1, P2, and P222 symmetries yielded neat fits to the experimental data (Figure 2A; the discrepancy values χ_s are given in Table 2), and the volumes of the models corresponded to those of tetrameric assemblies. The symmetry conditions do not worsen the quality of the fit, indicating that both constructs can possess P222 symmetry (expected for tetramers). Superposition of the FlRd and FDP shapes obtained in P222 (Figure 3) indicates that the two proteins have a similar overall structure. However, there is an extra volume on the periphery of FlRd, which can accommodate the Rd domains and linkers. This result is in agreement with the above analysis of the overall parameters and $p(r)$ functions. The shape reconstructions without symmetry restrictions yielded models similar to those in Figure 3. The similarity was confirmed using the automated matching program SUPCOMB (Kozin and Svergun, 2001), as the normalized spatial discrepancy (NSD) values between the models were below 0.8 (see Experimental Procedures for more details).

Rigid-Body Modeling

The ab initio shape of the tetrameric FDP core (Figure 3) resembles the crystallographic tetramer of *Moorella thermoacetica*

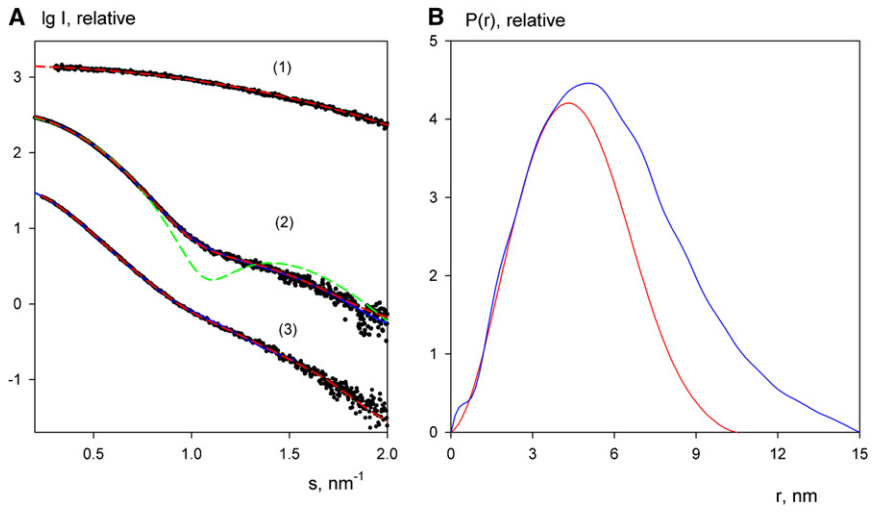

Figure 2. Scattering Patterns and Distribution Functions

(A) SAXS data of FlRd constructs. (1) Rd module, (2) FDP core, and (3) full-length FlRd. Experimental data are denoted by dots, and fits from ab initio and rigid-body models (homology model for Rd domain) are shown as blue solid and red dashed lines, respectively. The fit from the crystallographic tetramer (Figure 1B) of *M. thermoacetica* FDP is given as a green dashed line.

(B) Distance distribution functions of the FDP core (red) and full-length FlRd (blue).

FDP (Figure 1B) (which shares 41% sequence identity with FlRd). However, the scattering curve computed in CRYSOL (Svergun et al., 1995) from the atomic coordinates of the latter does not fit the experimental data (χ = 6.6; Figure 2A). This suggests that the tetrameric assembly is different in solution compared to that in the crystal. Given that the FDP dimer interface is necessary to maintain contacts between the diiron and FMN cofactors, the dimer interface was maintained intact when performing rigid-body modeling of FlRd. The positions of the dimers were refined assuming that they are identical in the FDP and FlRd tetramers. Rigid-body modeling was performed using the program SASREF (Petoukhov and Svergun, 2005) to build a model of the full-length FlRd tetramer by simultaneous fitting of the scattering curves from FDP and FlRd. Given that the homology model of the Rd domain is compatible with the experimental SAXS data, it was used for molecular modeling together with the crystallographic FDP dimer. First, the modeling was performed using P222 symmetry restrictions on the entire FlRd. In P222, the symmetrically independent entity is the FDP monomer and therefore distance restraints were imposed to maintain the dimer interface (see Experimental Procedures). Additional distance restraints were used to attach the linker and Rd domain to the C termini of the FDP monomers. Rigid-body modeling led to a significantly improved fit between the computed curves and the experimental data for FDP (χ = 2.0; Figure 2A). Interestingly, the resulting model had an almost parallel arrangement of the dimers (Figure 4A) in contrast to their tilted configuration in the crystallographic tetramer (Figure 1B). Such rearrangement corresponds to a screw movement, with 25° rotation and 0.25 nm outward shift of each dimer along the axis connecting the centers of the dimers yielding a root-mean-square deviation (rmsd) of 1.3 nm between the atoms of the original and the refined models. As expected, the Rd modules were located on the periphery of FlRd and showed loose interactions with the FDP core.

Table 2. Parameters Obtained by SAXS

Sample	I_0	R_g (nm)	V_p (nm^3)	D_{max} (nm)	χ_s	χ_{orig}	χ_{rb}
FlRd	387	4.5	375	15	1.36	-	1.0
FDP	342	3.4	330	10.5	1.58	6.6	2.0
Rd	14.6	1.2	10.2	3.5	-	1.4	-

I_0, R_g, V_p, and D_{max} are forward scattering, radius of gyration, excluded volume, and maximum size, respectively. χ_s and χ_{orig} are the discrepancies from the ab initio and atomic models (crystal structure for FDP and a homology model for Rd). χ_{rb} are the values from the typical rigid-body model reconstructed with no symmetry restrictions for the linker and Rd domain while keeping P222 for the FDP dimer.

The fact that the Rd modules were positioned far from the FDP core suggests high mobility and possible asymmetry in the linker and Rd portions. Further refinement with symmetry restrictions applied only to the FDP core and not to the four copies of the linker, and the Rd domain yielded a minor improvement in the fit to the experimental data for FlRd (Figure 2A). A typical asymmetric model is presented in Figure 4B and the corresponding χ values are given in Table 2. Other modeling attempts, without any symmetry restraints or assuming a single two-fold axis, produced models with similar overall shapes with the FDP core surrounded by distant Rd domains. However, compared to the symmetry-restrained calculations, these models did not improve the fits to the experimental SAXS data.

The ab initio model of FlRd in Figure 3 displays two (not four) extra bulges emerging from the FDP core, hinting at a possible interaction between pairs of Rd domains. This possibility was tested by rigid-body modeling (SASREF) in P222 with additional distance restraints to impose pairwise proximity of the Rd domains. A typical result from this modeling (Figure 4C) displays Rd-Rd contacts, but compared to the other two models in Figure 4 gives a worse fit to the experimental data. Thus, it can be concluded that the interaction of pairs of Rd domains is unlikely. The smaller bulges in the ab initio model result from its low resolution and the requirement of compactness. The highly extended linkers between the FDP and Rd domains in full-length FlRd are likely to be flexible, and therefore the models in Figure 4 are snapshots of the possible configurations of the Rd domains. Importantly, however, these extended configurations were reproducibly obtained in multiple reconstructions and they rule out tight contacts between the Rd domains and the FDP core.

Accessing Conformational Variability

In the above approaches, we tried to generate structural models fitting experimental scattering data on a "one-to-one" basis, that is, to find a single model which fits the experimental pattern. The results obtained demonstrate virtually no contacts between the

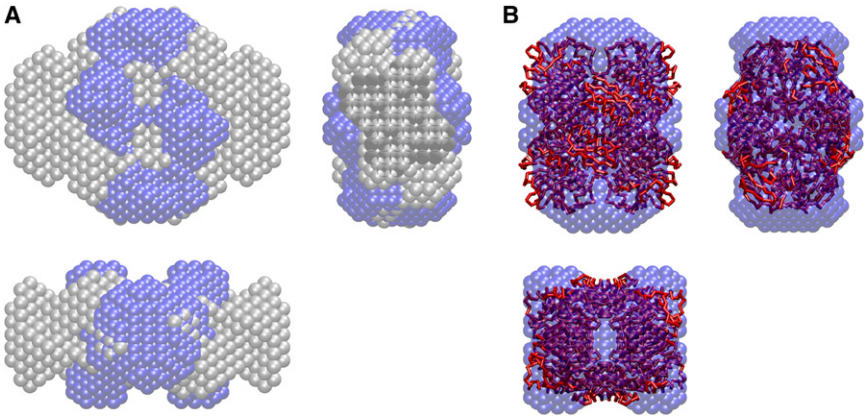

Figure 3. Ab Initio Modeling of FlRd Constructs
(A) Ab initio models of FlRd (gray beads) and the FDP core (blue beads) reconstructed in P222.
(B) Comparison of the ab initio shape of FDP with the crystallographic tetramer of of *M. thermoacetica* FDP (shown as a red backbone trace).

Rd domains and the FDP core (Figure 4). It is logical to expect high flexibility of the linkers and therefore of the positions of the Rd domains. To address this potential flexibility and to quantitatively describe the preferential positions of the C-terminal part of FlRd, a recently developed alternative modeling approach was used allowing for the coexistence of multiple conformations in solution. This approach, called the ensemble optimization method (EOM; Bernado et al., 2007), generates representative sets of randomized models and employs a genetic algorithm to select subsets of these models such that their averaged scattering fits the experimental data.

For EOM, the tetrameric FDP core was fixed in the arrangement taken from the best rigid-body model and the Rd domains in random orientations were attached to the core by random linkers. First, the pool was filled with 10,000 asymmetric models whereby the conformations and orientations of the four linkers in the tetramer were independent of one another. The R_g distribution of the models in this pool is displayed in Figure 5 (curve 1). Surprisingly, the optimization of this pool did not allow fitting of the experimental data, and even the best subensembles yielded χ worse than 4.0. Analysis of the R_g distribution in the selected ensembles indicated that EOM was trying to select models with R_g exceeding 4.2 nm, which were nearly absent in the asymmetrically generated pool. This indicated that the extent of the 10,000 random asymmetric models was insufficient to adequately sample the conformational space of FlRd. The use of P222 symmetry for the generation of the random pool of only 1,000 structures widened significantly the R_g distribution compared to the asymmetric case (Figure 5, curve 2) and EOM yielded better fits to the data with $\chi = 1.5$. The widening of the distribution in the symmetric case is explained by the cumulative effect of the linker conformations in each monomer (e.g., all linkers are either compacted or extended).

To further explore the possible asymmetry of FlRd, yet another 1,000 structures were generated without symmetry constraints but with the requirement of the extended conformation of the linkers (a minimum of 5.0 nm end-to-end distance). Note that this method of generation (with the R_g distribution in Figure 5, curve 3) still did not exclude the possibility of contacts between the Rd and FDP domains. The use of the entire pool of 12,000

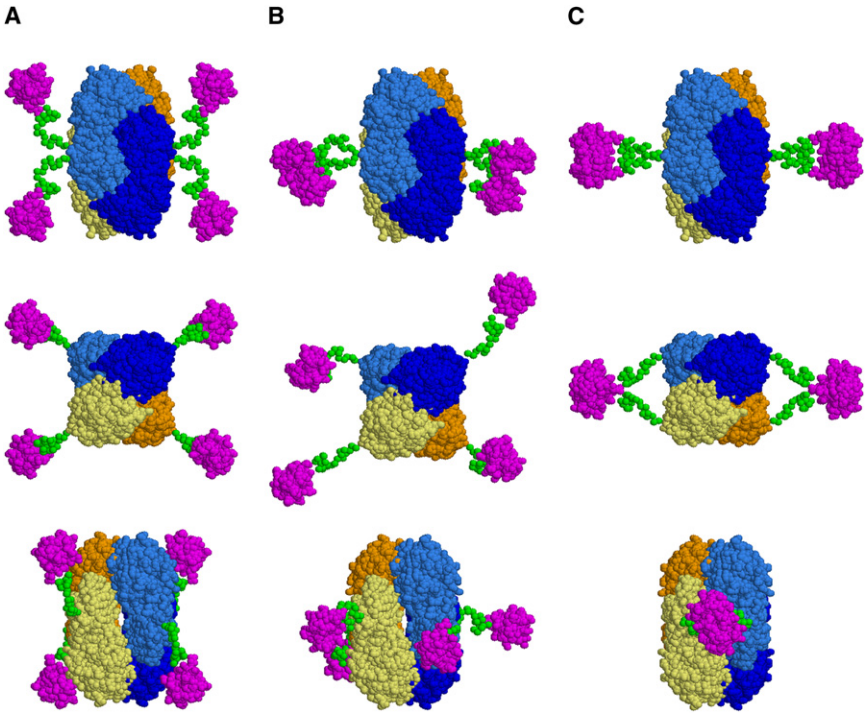

Figure 4. Rigid-Body Models of FlRd
(A) Reconstruction in P222.
(B) No symmetry restraints for the Rd domain and linkers.
(C) P222 modeling with the requirement of contacts between Rd domains.
These are displayed in space-filled mode with the same color scheme for the FDP tetramer as in Figure 1B. The linkers and Rd domain are colored green and magenta, respectively. The middle and bottom views are rotated by 90° about the horizontal and vertical axes, respectively.

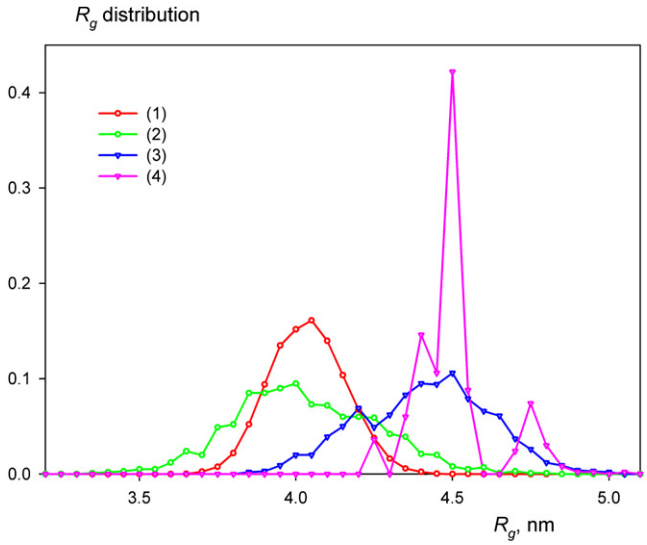

Figure 5. The Distributions of the Radii of Gyration in the Ensembles of FlRd

Pools containing the FDP core with four Rd domains attached by random linkers and consisting of 10,000 asymmetric structures (1), 1,000 symmetric structures (2), and 1,000 asymmetric models with extended linkers (3). Distribution (4) corresponds to the average over 150 ensembles selected by EOM.

random and deliberately extended models (both symmetric and asymmetric) yielded marginal improvement in the fit (χ = 1.3) compared to the purely symmetric case. Also, the fits obtained in multiple EOM runs were approximately of the same quality as that of the rigid-body model. However, the EOM provides the important result that in all selected models, all the linkers were significantly extended and the Rd domains were located far from the core and, moreover, not a single model showed contacts between any of the Rd domains and the core. The R_g distribution of the selected models is shifted significantly to the larger values compared to that of the pool (see Figure 5, curve 4). This finding suggests that the extended conformation of the linkers with no interactions between the Rd domains and the core is predominant in solution. A typical subset of selected structures giving the idea of structural diversity of FlRd is displayed in Figure 6. The average length of the linker between the FDP and Rd domains in the selected models was 4.3 ± 0.8 nm, close to the expected distance between the N and C termini of a 24 amino acid long random peptide (Fitzkee and Rose, 2004). The average rmsd between the atomic coordinates of the Rd domain in distinct models was 3.9 ± 1.6 nm, somewhat exceeding the diameter of the Rd molecule (about 3 nm). These average parameters further confirm that the Rd portions, although protruding far to the periphery of FlRd, occupy rather well defined sectors relative to the FDP core.

DISCUSSION

Protein-protein interactions are integral to protein function, as quaternary structure provides a framework for the juxtaposition of active sites. The analyses of protein crystal structures, and packing interfaces in particular, have yielded important insights into the determinants of oligomerization (Bahadur et al., 2004;

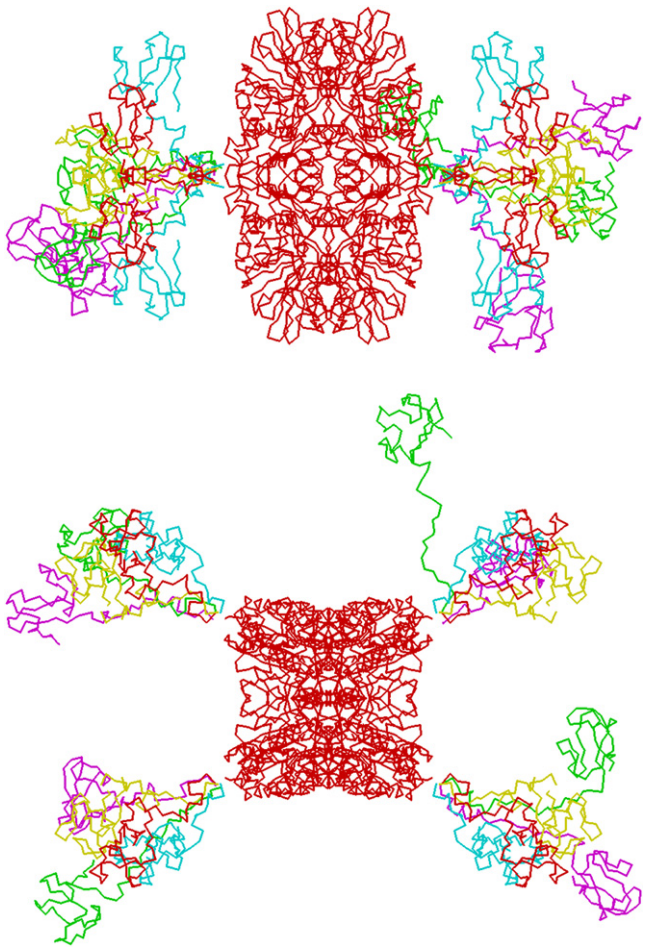

Figure 6. EOM Representative Models

A typical ensemble selected by EOM from a pool of randomized structures. The bottom view is rotated by 90° about horizontal axis.

Ponstingl et al., 2005). In the present paper, SAXS was employed to elucidate the structure of FlRd and to establish the relative position of the Rd module with respect to the FDP core. Both the FDP core and full-length FlRd were found to be tetrameric in solution, and removal of the Rd domain had little impact on this tetrameric assembly. Surprisingly, although the ab initio shape reconstruction of FDP appeared similar to the crystallographic tetramer of the homologous *M. thermoacetica* protein, the scattering pattern computed from this tetramer failed to fit the experimental SAXS data. For comparison, SAXS data were also obtained on Dg_ROO. This construct displayed some aggregation, which was reflected by an intensity upturn at very small angles (Figure 7), but starting from about s = 0.3 nm^{-1} (i.e., resolution about 20 nm) the experimental scattering from Dg_ROO neatly coincided with that from the FDP construct of FlRd. One can conclude that the tetrameric assembly of the FDPs is different in solution compared to that in the crystal. Whereas the "head-to-tail" dimer interface (which mediates close contacts between the diiron and FMN sites; Figure 1B) is likely to be maintained in solution, the dimer-dimer packing within the tetramer is altered (0.25 nm shift and 25° rotation of each dimer, as mentioned above). This difference is not

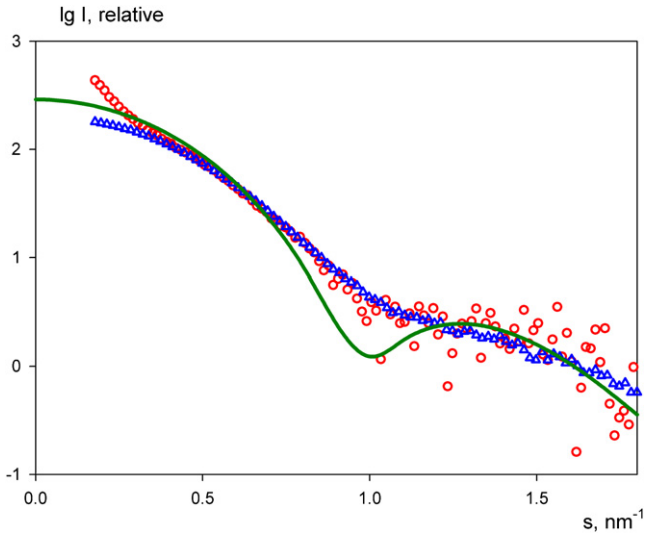

Figure 7. Comparison of the Experimental Scattering Profiles of Dg_ROO and FlRd

The scattering curve computed from the crystallographic Dg_ROO tetramer (PDB ID code 1YCH) is presented as a green solid line. Dg_ROO, red circles; FlRd, blue triangles.

surprising, as crystal packing forces can alter the quaternary structure of multisubunit proteins, which is reported in numerous publications (e.g., Andersen et al., 2006; Svergun et al., 2000).

To further understand the oligomeric organization of FDP, it should be recalled that four of its five crystal structures demonstrated the tetrameric assembly illustrated in Figure 1B. However, the structure of the homolog from *T. maritima* (PDB ID code 1VME) does not involve any large dimer-dimer interface, on account of an N-terminal His tag, which is sufficient to sterically hinder oligomerization. In addition to highlighting differences between the crystal and solution structure of FDPs, analysis of the SAXS data also reveals interesting information on the location and behavior of the Rd module. Deletion of the C-terminal Rd domain did not lead to any significant rearrangement of the FDP core. Both the ab initio and the rigid-body modeling indicate that the Rd domain is remotely positioned with respect to the core. Despite some ambiguities in the rigid-body analysis (which may partly be attributed to flexibility in the tetrameric assembly of FlRd), the Rd domains were consistently positioned on the periphery of FlRd and displayed weak contacts with the FDP core (Figures 4 and 6). It appears therefore that the Rd domain of FlRd is tethered by a flexible linker and exhibits considerable configurational freedom. Extensive domain motions are known to be important in a number of redox systems. For example, in the cytochrome bc_1 complex, the Rieske protein has a flexible tether and moves through a distance of ~15 Å to transfer electrons from cytochrome *b* to cytochrome c_1 (Zhang et al., 1998). The FAD domain of the modular electron-transferring flavoprotein is also known to explore different conformations to facilitate electron transfer to redox partners (Leys et al., 2003). Moreover, NMR studies have revealed examples of transient redox complexes in which the proteins form a dynamic ensemble of energetically similar configurations (Volkov et al., 2005; Worrall et al., 2002, 2003).

In the rigid-body modeling of the FlRd structures, we employed the atomic structure of *M. thermoacetica* FDP (PDB ID code 1YCH) yielding the best sequence homology to FlRd among the models available from the Protein Data Bank. To verify whether minor changes in the atomic structure of the template would have an impact on the results, we screened five monomeric structures of FDP from the PDB. As the sequence homology may not necessarily correlate with the structural homology, we first compared the scattering patterns computed from the five monomers (see Figure S1 available online). The monomers gave very similar scattering in the range of scattering angles responsible for the quaternary structure of FlRd (up to $s = 2\ nm^{-1}$). Then we took the monomer of F420H2 oxidase (PDB ID code 2OHH) yielding the largest discrepancy to the scattering computed from PDB ID code 1YCH and performed rigid-body modeling using the monomeric PDB ID code 2OHH structure. The generated model of the FlRd core based on the PDB ID code 2OHH monomer yields a somewhat worse fit to the experimental SAXS data (Figure S2) but shows virtually the same arrangement of dimers in the FlRd core tetramer as the model reported in the paper (Figure S3). This indicates that minor variations in the tertiary structure of the monomeric template have little impact on the overall model of the FlRd core.

The analysis of crystallographic and NMR spectroscopic data indicates that redox proteins form transient complexes via small flat binding sites (~500 $Å^2$ buried surface per protein), the core of which is hydrophobic and encompasses the redox cofactor or a surface-exposed ligand of the active site (Crowley and Carrondo, 2004; Crowley and Ubbink, 2003). Polar and charged side chains line the periphery of the binding site and frequently there is a juxtaposition of complementary charged groups across the interface. This type of binding site architecture was found recently in the crystal structure of a rubredoxin bound to its reductase (Hagelueken et al., 2007). Acidic patches flanking the Fe-Cys_4 site of Rd are complemented by clusters of basic side chains that surround the exposed edge of the FAD isoalloxazine ring in rubredoxin reductase. Interestingly, a similar portion of the FMN group (atom N3 of the isoalloxazine ring) protrudes through the "back" of FlRd, and the surrounding surface is positively charged (Figure 8A). Previous protein-docking simulations of the interaction between rubredoxin and Dg_ROO identified this region of the protein surface as the putative Rd binding site (Victor et al., 2003). It can be envisaged that coulombic attractions between this positive patch and the negatively charged Rd (as putatively illustrated in Figure 8) steer the mobile Rd domain toward redox active interactions with the FMN site of FDP. Moreover, the linker is sufficiently long as to permit Rd access to this region of the FDP core (Victor et al., 2003).

The SAXS data herein reported complement previous biochemical studies on the electron transfer reaction between FlRd and FlRd reductase. Electron transfer from FlRd reductase involves the Rd domain as the electron entry point of FlRd. Subsequently, electrons are shuttled via intramolecular steps to the FMN and then to the diiron center, where reduction of NO is catalyzed (Vicente et al., 2007; Vicente and Teixeira, 2005). There is evidence (both from UV/vis spectroscopy and gel-permeation chromatography) for complex formation between FlRd and its reductase (Vicente and Teixeira, 2005), and the presence of the reductase modulates the reduction potentials of the iron centers in FlRd: the

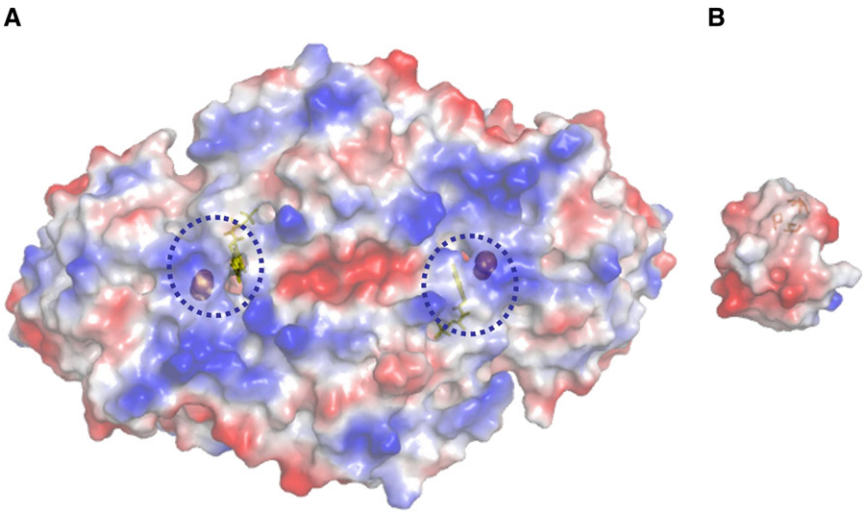

Figure 8. Electrostatic Potentials of FDP and Rd

Structural models of (A) the FDP core and (B) the Rd module of FlRd, built in SWISS-MODEL (Arnold et al., 2006) using the structures of *M. thermoacetica* FDP (PDB ID code 1YCH; Silaghi-Dumitrescu et al., 2003) and *C. pasteurianum* rubredoxin (PDB ID code 4RXN; (Watenpaugh et al., 1980). The dashed circles indicate the approximate location of the FMN and diiron cofactors in FDP. The surface maps were generated using PyMOL (DeLano, 2002).

Fe-Cys_4 in the Rd domain and the diiron site in the lactamase domain. This indicates that the binding interface between FlRd and FlRd reductase involves the Rd domain. Redox modulation of the diiron center could arise either through binding of the reductase (near the diiron center) or docking of the Rd domain (Figure 8).

The kinetics of the electron transfer reaction with FlRd reductase has been investigated for full-length FlRd and for the independent Rd module (Vicente et al., 2007). It was observed that the reduction of the Fe-Cys_4 center (in the Rd domain) and the FMN (in the FDP core) are kinetically synchronous and the electron transfer rates both display a linear dependence on the reductase concentration. This is an important observation, considering that reduction of FMN by the Fe-Cys_4 of Rd is an intramolecular step. Moreover, it was proposed that four electrons entering FlRd at the Rd domain are quickly equilibrated through the redox cofactors. The Fe-Cys_4 center in the Rd domain is a one-electron acceptor/donor, whereas the redox and kinetic properties of the reductase attest that it quickly and sequentially donates two electrons without accumulation of the partially reduced FAD semiquinone. It was also found that the ionic strength dependence of the reaction between the reductase and the Rd domain as a truncated independent protein or as part of the full-length FlRd displays similar profiles. The fact that the long-range electrostatic contribution to the reaction with FlRd reductase is similar whether the Rd domain is independent or tethered (as in FlRd) suggests that Rd is weakly associated with the core domains of FlRd. To comply with these features of the electron transfer process, it is envisaged that the Rd domain is loosely accommodated at the binding interface between FlRd and FlRd reductase. The SAXS data reveal the Rd domain to be sufficiently flexible as to serve as a one-electron shuttle between FlRd reductase and the FDP core of FlRd.

In summary, the quaternary structure of FlRd as revealed by SAXS consists of a dimer of dimers with peripheral Rd domains (Figures 4 and 6). Despite the presence of a linker and the concomitant "concentration effect," the Rd module behaves as an independent domain with sufficient mobility to shuttle electrons from FlRd reductase to the FMN of the FDP core from where they are transferred to the NO-reducing diiron site, thus mimicking the situation of the two-domain FDPs which have mobile rubredoxins as immediate electron donor proteins.

EXPERIMENTAL PROCEDURES

Sample Preparation

Samples of FlRd and its truncated domains were obtained as previously described (Gomes et al., 2002; Vicente and Teixeira, 2005) (Table 1). Each protein was further washed through a PD-10 (Amersham) gel-filtration column to exchange the buffer to 50 mM Tris-HCl, 18% glycerol (pH 7.5). Protein concentrations were determined both by the bicinchoninic acid method (Brown et al., 1989) and visible absorption spectroscopy using known molar extinction coefficients (Gomes et al., 2000; Vicente et al., 2007). The bicinchoninic acid assay was used to complement the quantification by UV/visible spectroscopy (based on specific molar extinction coefficients), which only accounts for fully loaded protein in terms of optically active redox cofactors.

SAXS Data Collection and Processing

Synchrotron X-ray scattering data from solutions of the Rd domain, the FDP core, and full-length FlRd were collected at the X33 beamline (DESY, Hamburg, Germany) (Roessle et al., 2007) using a MAR345 image plate detector. The scattering patterns of all samples were measured at several solute concentrations c, ranging from 2 to 5.0 mg/ml. At a sample-detector distance of 2.7 m, the range of momentum transfer $0.1 < s < 5$ nm^{-1} was covered ($s = 4\pi \sin[\theta]/\lambda$, where 2θ is the scattering angle and $\lambda = 0.15$ nm is the X-ray wavelength). The data were processed using standard procedures in the program package PRIMUS (Konarev et al., 2003). The forward scattering I_0 and the radii of gyration R_g were evaluated using the Guinier approximation (Guinier, 1939), assuming that at very small angles ($s < 1.3/R_g$), the intensity is represented as $I(s) = I_0 \exp(-[sR_g]^2/3)$. The maximum dimensions D_{max} were computed using the indirect transform package GNOM (Svergun, 1992), which also provides the distance distribution functions $p(r)$.

The increase in molecular mass (MM) of the full-length FlRd compared to the shorter construct was verified by the analysis of the forward scattering value I_0 using the proportion MM $\sim I_0/c$. In addition, the excluded (Porod) volumes V_p of the solutes were also analyzed, calculated as (Porod, 1982)

$$V = 2\pi^2 I(0) / \int_0^\infty s^2 I(s) ds. \quad (1)$$

In this calculation, an appropriate constant was subtracted from each data point to force an s^{-4} decay of the intensity at higher angles following Porod's law (Porod, 1982) for homogeneous particles. For globular proteins, Porod (i.e., hydrated) volumes in nm^3 are approximately twice the MMs in kDa.

Ab Initio Shape Determination

Low-resolution shape analysis of the solutes was performed using the ab initio program DAMMIN (Svergun, 1999), which represents the macromolecule by an assembly of densely packed beads. Simulated annealing (SA) is employed to build a compact interconnected configuration of beads inside a sphere with the diameter D_{max} that fits the experimental data $I_{exp}(s)$ to minimize the discrepancy χ:

$$\chi^2 = \frac{1}{N-1} \sum_j \left[\frac{I_{exp}(s_j) - cI_{calc}(s_j)}{\sigma(s_j)} \right]^2, \quad (2)$$

where N is the number of experimental points, c is a scaling factor, and $I_{calc}(s)$ and $\sigma(s_j)$ are the calculated intensity and the experimental error at the momentum transfer s_j, respectively. The shape reconstructions of FDP and FlRd were made assuming no symmetry and also with P1, P2, and P222 symmetry constraints.

Molecular Modeling

The program SASREF (Petoukhov and Svergun, 2005) was employed for molecular modeling of the FDP core and the full-length FlRd based on the atomic model of *M. thermoacetica* FDP (PDB ID code 1YCH; Silaghi-Dumitrescu et al., 2005a; which of the known FDP structures is closest in sequence identity [41%] to FlRd) and a homology model of the Rd domain (~55 residues) built in SWISS-MODEL using the coordinates of *Clostridium pasteurianum* rubredoxin (PDB ID code 4RXN) as a template (Arnold et al., 2006). The linker between the FDP and Rd domains was represented by a randomly generated self-avoiding C_α backbone of 24 amino acids with proper bond and dihedral angles. SASREF uses SA to position the domains with respect to each other, forming an interconnected assembly without steric clashes while minimizing the discrepancy between the experimental data and the scattering profiles computed from both the full-length model and the FDP core. The model scattering is calculated based on the precomputed partial amplitudes of the subunits in the reference positions and orientations. The scattering from the atomic models was calculated using the program CRYSOL (Svergun et al., 1995), which either predicts theoretical scattering patterns or fits the experimental data by adjusting the excluded volume and the contrast of the hydration layer. Distance restraints were applied to ensure the contacts between the linker and the appropriate termini of the domains yielding an interconnected chain (spring force potential was used as described in Petoukhov and Svergun, 2005). Rigid-body modeling was performed using P222 symmetry constraints. Distance restraints between the FDP monomers (His115-Trp376, Met262-Gly26, Ser84-Trp263, and Gly331-Asp317) were applied to maintain the dimer interface as in PDB ID code 1YCH.

For ab initio and rigid-body analysis, multiple runs were performed to verify the stability of the solution, and the most typical reconstructions were selected using the programs DAMAVER (Volkov and Svergun, 2003) and SUPCOMB (Kozin and Svergun, 2001). The latter program aligns two arbitrary low- or high-resolution models represented by ensembles of points by minimizing a dissimilarity measure called normalized spatial discrepancy (NSD). For every point (bead or atom) in the first model, the minimum value among the distances between this point and all points in the second model is found, and the same is done for points in the second model. These distances are added and normalized against the average distances between the neighboring points for the two models. Generally, NSD values close to unity indicate that the two models are similar. The program DAMAVER generates the average model of the set of superimposed structures and also specifies the most typical model (i.e., that having the lowest average NSD with all the other models of the set).

Ensemble Optimization Method

The conformational space of FlRd was explored using the recently developed EOM approach, which takes flexibility into account by allowing for the coexistence of multiple conformations in solution (Bernado et al., 2007). EOM selects appropriate ensembles of configurations from large pools of random models of the protein. Even when a single model gives a reasonable fit, EOM allows one to assess the range of different conformations which the flexible protein can potentially adopt. Representative models were created by random generation of the loops connecting Rd domains to the FDP core. The theoretical scattering intensities of the randomized models were calculated using the program CRYSOL (Svergun et al., 1995). The program GAJOE from the EOM package (Bernado et al., 2007) employed a genetic algorithm to select from the pool of structures the ensembles of curves (and subsequent 3D models) such that the averages over the ensembles fitted the experimental data while minimizing the discrepancy χ (Equation 2). By running EOM multiple times it is also possible to compare the R_g distributions of the selected structures versus the original pool.

SUPPLEMENTAL DATA

Supplemental Data include three figures and can be found with this article online at http://www.structure.org/cgi/content/full/16/9/1428/DC1/.

ACKNOWLEDGMENTS

M.V.P. and D.I.S. acknowledge support from the EU design study SAXIER (contract RIDS 011934). P.B.C. acknowledges funding from the Marie Curie Foundation (Fifth Framework Programme, HPMF-CT-2002-02008) and the EU (I3 travel grant). M.T. and J.B.V. acknowledge funding from Fundação para a Ciência e Tecnologia, respectively, for project grants POCTI/2002/BME/44597 and PTDC/BIA-PRO/67263/2006 and PhD grant SFRH/BD/9136/2002.

Received: December 20, 2007
Revised: June 1, 2008
Accepted: June 3, 2008
Published: September 9, 2008

REFERENCES

Andersen, C.B., Becker, T., Blau, M., Anand, M., Halic, M., Balar, B., Mielke, T., Boesen, T., Pedersen, J.S., Spahn, C.M., et al. (2006). Structure of eEF3 and the mechanism of transfer RNA release from the E-site. Nature *443*, 663–668.

Andersson, J.O., Hirt, R.P., Foster, P.G., and Roger, A.J. (2006). Evolution of four gene families with patchy phylogenetic distributions: influx of genes into protist genomes. BMC Evol. Biol. *6*, 27.

Arnold, K., Bordoli, L., Kopp, J., and Schwede, T. (2006). The SWISS-MODEL workspace: a web-based environment for protein structure homology modelling. Bioinformatics *22*, 195–201.

Bahadur, R.P., Chakrabarti, P., Rodier, F., and Janin, J. (2004). A dissection of specific and non-specific protein-protein interfaces. J. Mol. Biol. *336*, 943–955.

Bernado, P., Mylonas, E., Petoukhov, M.V., Blackledge, M., and Svergun, D.I. (2007). Structural characterization of flexible proteins using small-angle X-ray scattering. J. Am. Chem. Soc. *129*, 5656–5664.

Brown, R.E., Jarvis, K.L., and Hyland, K.J. (1989). Protein measurement using bicinchoninic acid: elimination of interfering substances. Anal. Biochem. *180*, 136–139.

Chen, L., Liu, M.Y., LeGall, J., Fareleira, P., Santos, H., and Xavier, A.V. (1993). Rubredoxin oxidase, a new flavo-hemo-protein, is the site of oxygen reduction to water by the "strict anaerobe" *Desulfovibrio gigas*. Biochem. Biophys. Res. Commun. *193*, 100–105.

Crowley, P.B., and Ubbink, M. (2003). Close encounters of the transient kind: protein interactions in the photosynthetic redox chain investigated by NMR spectroscopy. Acc. Chem. Res. *36*, 723–730.

Crowley, P.B., and Carrondo, M.A. (2004). The architecture of the binding site in redox protein complexes: implications for fast dissociation. Proteins *55*, 603–612.

DeLano, W.L. (2002). The PyMOL Molecular Graphics System (http://www.pymol.org/).

Di Matteo, A., Scandurra, F.M., Testa, F., Forte, E., Sarti, P., Brunori, M., and Giuffre, A. (2008). The O_2-scavenging flavodiiron protein in the human parasite *Giardia intestinalis*. J. Biol. Chem. *283*, 4061–4068.

Feigin, L.A., and Svergun, D.I. (1987). Structure Analysis by Small-Angle X-Ray and Neutron Scattering (New York: Plenum Press).

Fitzkee, N.C., and Rose, G.D. (2004). Reassessing random-coil statistics in unfolded proteins. Proc. Natl. Acad. Sci. U.S.A. *101*, 12497–12502.

Frazao, C., Silva, G., Gomes, C.M., Matias, P., Coelho, R., Sieker, L., Macedo, S., Liu, M.Y., Oliveira, S., Teixeira, M., et al. (2000). Structure of a dioxygen reduction enzyme from *Desulfovibrio gigas*. Nat. Struct. Biol. *7*, 1041–1045.

Gomes, C.M., Silva, G., Oliveira, R., LeGall, J., Liu, M.-Y., Xavier, A.V., Rodrigues-Pousada, C., and Teixeira, M. (1997). Studies on the redox centers of the terminal oxidase from *Desulfovibrio gigas* and evidence for its interaction with rubredoxin. J. Biol. Chem. *272*, 22502–22508.

Gomes, C.M., Vicente, J.B., Wasserfallen, A., and Teixeira, M. (2000). Spectroscopic studies and characterization of a novel electron-transfer chain from *Escherichia coli* involving a flavorubredoxin and its flavoprotein reductase partner. Biochemistry *39*, 16230–16237.

Gomes, C.M., Giuffre, A., Forte, E., Vicente, J.B., Saraiva, L.M., Brunori, M., and Teixeira, M. (2002). A novel type of nitric-oxide reductase. *Escherichia coli* flavorubredoxin. J. Biol. Chem. *277*, 25273–25276.

Guinier, A. (1939). La diffraction des rayons X aux tres petits angles; application a l'etude de phenomenes ultramicroscopiques. Ann. Phys. (Paris) *12*, 161–237.

Hagelueken, G., Wiehlmann, L., Adams, T.M., Kolmar, H., Heinz, D.W., Tummler, B., and Schubert, W.D. (2007). Crystal structure of the electron transfer complex rubredoxin rubredoxin reductase of *Pseudomonas aeruginosa*. Proc. Natl. Acad. Sci. USA *104*, 12276–12281.

Konarev, P.V., Volkov, V.V., Sokolova, A.V., Koch, M.H.J., and Svergun, D.I. (2003). PRIMUS—a Windows-PC based system for small-angle scattering data analysis. J. Appl. Crystallogr. *36*, 1277–1282.

Kozin, M.B., and Svergun, D.I. (2001). Automated matching of high- and low-resolution structural models. J. Appl. Crystallogr. *34*, 33–41.

Leys, D., Basran, J., Talfournier, F., Sutcliffe, M.J., and Scrutton, N.S. (2003). Extensive conformational sampling in a ternary electron transfer complex. Nat. Struct. Biol. *10*, 219–225.

Petoukhov, M.V., and Svergun, D.I. (2005). Global rigid body modelling of macromolecular complexes against small-angle scattering data. Biophys. J. *89*, 1237–1250.

Ponstingl, H., Kabir, T., Gorse, D., and Thornton, J.M. (2005). Morphological aspects of oligomeric protein structures. Prog. Biophys. Mol. Biol. *89*, 9–35.

Porod, G. (1982). General theory. In Small-Angle X-Ray Scattering, O. Glatter and O. Kratky, eds. (London: Academic Press), pp. 17–51.

Rodrigues, R., Vicente, J.B., Felix, R., Oliveira, S., Teixeira, M., and Rodrigues-Pousada, C. (2006). *Desulfovibrio gigas* flavodiiron protein affords protection against nitrosative stress in vivo. J. Bacteriol. *188*, 2745–2751.

Roessle, M.W., Klaering, R., Ristau, U., Robrahn, B., Jahn, D., Gehrmann, T., Konarev, P., Round, A., Fiedler, S., Hermes, C., and Svergun, D. (2007). Upgrade of the small-angle X-ray scattering beamline X33 at the European Molecular Biology Laboratory, Hamburg. J. Appl. Crystallogr. *40*, S190–S194.

Saraiva, L.M., Vicente, J.B., and Teixeira, M. (2004). The role of the flavodiiron proteins in microbial nitric oxide detoxification. Adv. Microb. Physiol. *49*, 77–129.

Sarti, P., Fiori, P.L., Forte, E., Rappelli, P., Teixeira, M., Mastronicola, D., Sanciu, G., Giuffre, A., and Brunori, M. (2004). *Trichomonas vaginalis* degrades nitric oxide and expresses a flavorubredoxin-type protein: a new pathogenic mechanism? Cell. Mol. Life Sci. *61*, 618–623.

Seedorf, H., Hagemeier, C.H., Shima, S., Thauer, R.K., Warketin, E., and Ermler, U. (2007). Structure of coenzyme F420H2 oxidase (FprA) a di-iron flavoprotein from methanogenic Archaea catalyzing the reduction of O_2 to H_2O. FEBS J. *274*, 1588–1599.

Silaghi-Dumitrescu, R., Coulter, E.D., Das, A., Ljungdahl, L.G., Jameson, G.N., Huynh, B.H., and Kurtz, D.M., Jr. (2003). A flavodiiron protein and high molecular weight rubredoxin from *Moorella thermoacetica* with nitric oxide reductase activity. Biochemistry *42*, 2806–2815.

Silaghi-Dumitrescu, R., Kurtz, D.M., Jr., Ljungdahl, L.G., and Lanzilotta, W.N. (2005a). X-ray crystal structures of *Moorella thermoacetica* FprA. Novel diiron site structure and mechanistic insights into a scavenging nitric oxide reductase. Biochemistry *44*, 6492–6501.

Silaghi-Dumitrescu, R., Ng, K.Y., Viswanathan, R., and Kurtz, D.M., Jr. (2005b). A flavo-diiron protein from *Desulfovibrio vulgaris* with oxidase and nitric oxide reductase activities. Evidence for an in vivo nitric oxide scavenging function. Biochemistry *44*, 3572–3579.

Svergun, D.I. (1992). Determination of the regularization parameter in indirect-transform methods using perceptual criteria. J. Appl. Crystallogr. *25*, 495–503.

Svergun, D.I. (1999). Restoring low resolution structure of biological macromolecules from solution scattering using simulated annealing. Biophys. J. *76*, 2879–2886.

Svergun, D.I., Barberato, C., and Koch, M.H.J. (1995). CRYSOL—a program to evaluate X-ray solution scattering of biological macromolecules from atomic coordinates. J. Appl. Crystallogr. *28*, 768–773.

Svergun, D.I., Petoukhov, M.V., Koch, M.H.J., and Koenig, S. (2000). Crystal versus solution structures of thiamine diphosphate-dependent enzymes. J. Biol. Chem. *275*, 297–302.

Vicente, J.B., and Teixeira, M. (2005). Redox and spectroscopic properties of the *Escherichia coli* nitric oxide-detoxifying system involving flavorubredoxin and its NADH-oxidizing redox partner. J. Biol. Chem. *280*, 34599–34608.

Vicente, J.B., Scandurra, F.M., Rodrigues, J.V., Brunori, M., Sarti, P., Teixeira, M., and Giuffre, A. (2007). Kinetics of electron transfer from NADH to the *Escherichia coli* nitric oxide reductase flavorubredoxin. FEBS J. *274*, 677–686.

Vicente, J.B., Carrondo, M.A., Teixeira, M., and Frazão, C. (2008). Flavodiiron proteins: nitric oxide and/or oxygen reductases. In Handbook of Metalloproteins, *Volume 4* (New York: Wiley)., in press.

Victor, B.L., Vicente, J.B., Rodrigues, R., Oliveira, S., Rodrigues-Pousada, C., Frazao, C., Gomes, C.M., Teixeira, M., and Soares, C.M. (2003). Docking and electron transfer studies between rubredoxin and rubredoxin:oxygen oxidoreductase. J. Biol. Inorg. Chem. *8*, 475–488.

Volkov, V.V., and Svergun, D.I. (2003). Uniqueness of ab initio shape determination in small angle scattering. J. Appl. Crystallogr. *36*, 860–864.

Volkov, A.N., Ferrari, D., Worrall, J.A.R., Bonvin, A.M., and Ubbink, M. (2005). Solution structure and dynamics of the complex between cytochrome *c* and cytochrome *c* peroxidase determined by paramagnetic NMR. Protein Sci. *14*, 799–811.

Wasserfallen, A., Ragettli, S., Jouanneau, Y., and Leisinger, T. (1998). A family of flavoproteins in the domains Archaea and Bacteria. Eur. J. Biochem. *254*, 325–332.

Watenpaugh, K.D., Sieker, L.C., and Jensen, L.H. (1980). Crystallographic refinement of rubredoxin at 1 × 2 Å degrees resolution. J. Mol. Biol. *138*, 615–633.

Worrall, J.A.R., Liu, Y., Crowley, P.B., Nocek, J.M., Hoffman, B.M., and Ubbink, M. (2002). Myoglobin and cytochrome b_5: a nuclear magnetic resonance study of a highly dynamic protein complex. Biochemistry *41*, 11721–11730.

Worrall, J.A.R., Reinle, W., Bernhardt, R., and Ubbink, M. (2003). Transient protein interactions studied by NMR spectroscopy: the case of cytochrome *c* and adrenodoxin. Biochemistry *42*, 7068–7076.

Zhang, Z., Huang, L., Shulmeister, V.M., Chi, Y.I., Kim, K.K., Hung, L.W., Crofts, A.R., Berry, E.A., and Kim, S.H. (1998). Electron transfer by domain movement in cytochrome bc_1. Nature *392*, 677–684.

